ELSEVIER

Journal of Structural Geology 27 (2005) 1143–1154

JOURNAL OF STRUCTURAL GEOLOGY

www.elsevier.com/locate/jsg

A viscoelastic strain energy principle expressed in fold–thrust belts and other compressional regimes

Regan L. Patton*, A. John Watkinson

Department of Geology, Washington State University, Pullman, WA 99164-2812, USA

Received 8 April 2003; received in revised form 2 April 2004; accepted 2 April 2004
Available online 12 October 2004

Abstract

A mathematical folding theory for stratified viscoelastic media in layer parallel compression is presented. The second order fluid, in slow flow, is used to model rock rheological behavior because it is the simplest nonlinear constitutive equation exhibiting viscoelastic effects. Scaling and non-dimensionalization of the model system reveals the presence of Weissenberg number (Wi), defined as a ratio of time scales $\tau^*/(H^*/V^*)$. V^*/H^* is the strain rate (s^{-1}) imposed by an assumed far field velocity V^* acting on a layer of thickness H^*, while τ^* (s) is related to the relaxation of normal stresses. Our most significant finding is a transitional behavior as $Wi \rightarrow ½$, which is independent of the viscosity contrast. A change of variables shows that lengths associated with this transition are scaled by a parameter $\alpha = [(1-2Wi)/(1+2Wi)]^{1/2}$, which is inversely proportional to local strain energy. On this basis a scaling law representing a distribution of non-dimensional wavelengths (wavelength/layer thickness) is derived. Geologically this is consistent with a transition from folding to faulting, as observed in fold–thrust belts. Folding, a distributed deformation scaling as Wi^{-1}, is found to be energetically favored at non-dimensional wavelengths ranging from about three to seven. Furthermore, the transition from folding to faulting, a localized deformation scaling as $(\alpha Wi)^{-1}$, is predicted at a non-dimensional wavelength of about seven. These findings are consistent with measurements of thrust sheets in the Sawtooth Mountains of western Montana, USA and other fold–thrust belts. A review of the literature reveals a similar distribution of non-dimensional wavelengths spanning a wide range of observational scales in compressional deformation. Specific examples include lithospheric scale folding in the central Indian Basin and microscopic scale failure of ice columns between splay microcracks in laboratory studies.

Keywords: Viscoelastic strain energy principle; Fold–thrust belts; Layer parallel compression; Rheological behavior

1. Introduction

Many naturally deformed rocks appear to have undergone complicated deformation histories. Inferring systematic narratives of deformation for given rock sequences requires detailed knowledge of the deformed state across a wide range of scales, as well as knowledge of the mechanical processes by which rocks deform. While technical skill in mapping deformation has increased dramatically over the past half-century, progress in understanding the mechanics of deformation has been somewhat limited. This is due in part to the kinematically restricted nature of most laboratory tests used to characterize rock behavior (Hobbs, 1972) and the uncertainty in extrapolating the resulting deformation mechanisms to geological conditions (Paterson, 1987; Rutter and Brodie, 1991). Nevertheless it is well known that rocks behave neither as purely viscous nor elastic media, but rather exhibit a wide range of behaviors including stress relaxation that might collectively be called 'viscoelastic'. For example, recent advances in laboratory rock mechanics have identified viscoelastic properties of rocks that are relevant to seismic wave attenuation and dispersion (Jackson, 2000). However, it is not clear how these data are relevant to deformation on the longer time scales assumed for orogenesis. Consequently, models provide a necessary means of connecting the spatial and temporal aspects of deformation, and can lead to the identification of useful principles for interpreting the deformed state. The purpose of this paper is to set forth such a principle on the foundation of observations in

* Corresponding author.
E-mail address: rpatton@theofficenet.com (R.L. Patton).

0191-8141/$ - see front matter © 2004 Elsevier Ltd. All rights reserved.
doi:10.1016/j.jsg.2004.08.007

fold–thrust belts and other compressional regimes spanning a wide range of scales.

Two potential explanations for the spatial complexity of deformation observed in outcrop are: (i) changes in material properties through time, and (ii) spatiotemporal, but not necessarily co-eval, complexities in the mechanisms of deformation. Certainly, there are well-documented examples of the former where through, for example, burial and subsequent exhumation rocks exhibit distinctive patterns of 'ductile' and overprinted 'brittle' deformation. In this case the familiar mechanical concepts of flow and fracture, and endmember constitutive models for 'viscous' and 'elastic' behaviors, have been applied with success. Just as certainly, however, there are cases where it is not clear that distinct deformation 'phases' occurred, yet the deformation is quite complex. We focus initially on a particular example of this found in a sandstone–shale sequence exposed along the Sun River near Augusta, Montana in the foreland disturbed belt of the Sawtooth Mountains. There, folds and faults occur together in a shallow crustal regime, but the faults do not all appear to postdate the folds. These observations raise questions regarding what constitutes an appropriate constitutive equation describing rock deformation in fold–thrust belts.

2. North Fork Sun River, Sawtooth Mountains

A striking feature of the disturbed belt in the Sawtooth Mountains, Montana is the large-scale, regularly spaced thrusts that repeat Paleozoic and lower Mesozoic sedimentary rocks (Mudge, 1972). A view from the air (Fig. 1) shows the repetition of thrust slices of predominantly Mississippian Madison Group limestones and dolomites in the frontal thrusts, typically thrust over Jurassic or Cretaceous shales. Estimation of the ratio of thrust slice length to bed thickness is dependent on the extrapolation to the unexposed cut-offs at depth and eroded cut-offs in the air. Without drill-hole data and seismic profiles, these estimates depend crucially on the geometric 'rule' used in the extrapolation (cf. Mudge (1972) with Mitra (1986)). The regularity of the outcrop distribution of the units does, however, imply the probability of some regularity of fault spacing, presumably related to bed thickness.

There is folding associated with these thrust plates, but the scale and exposure make it difficult to assess the relationship between faulting and folding. However, within the major thrust slices, a smaller-scale series of thrusts occur in the alternating sandstones and shales of Cretaceous age. These are closely associated with folds and are much better exposed. We have examined the folds and faults in these outcrops and measured the spacing of these structures at several scales.

We concentrate on smaller-scale exposures (tens of meters) that show more completely exposed thrust slices. One of the best of these occurs in the banks of the North Fork Sun River, east of the Diversion Thrust. Fig. 2 shows a portion of the outcrop with a sequence of thrusts and folds in a multilayered sandstone within a shale matrix (Johnson, 1988). Particular attention was given to the interrelationship between the faults and the folds, (i.e. Is the thrust slice folded? Does the fault occur on the limbs of a fold? What is the location and span of the fold with respect to a thrust?), and the distribution of non-dimensional fold and thrust wavelengths. The wavelength of a fold or thrust was first measured along the layer, and then divided by the thickness of the layer.

Fig. 1. Aerial photograph of the Sawtooth Mountains, showing regularly spaced thrust slices. Each cliff front marks a separate thrust sheet.

There are different styles of folds. The most dramatic are chevron folds with essentially parallel limbs and initial spans between about two and three. An initial span is defined as the length measured along the layer from one inflection point to the next on the adjacent limb (i.e. a half wavelength), divided by layer thickness. The chevron folds have more uniform limb thicknesses, in contrast to some other folds, which at fault cutoffs have a sheared limb appearance. While many of the fault cut-off zones have sheared limb folds, other folds exhibit sheared limbs without a fault offset, or with only a very small fault offset. Finally some of the thrust slices appear to be folded up against one another, forming complex zones of folded fault 'wedges'.

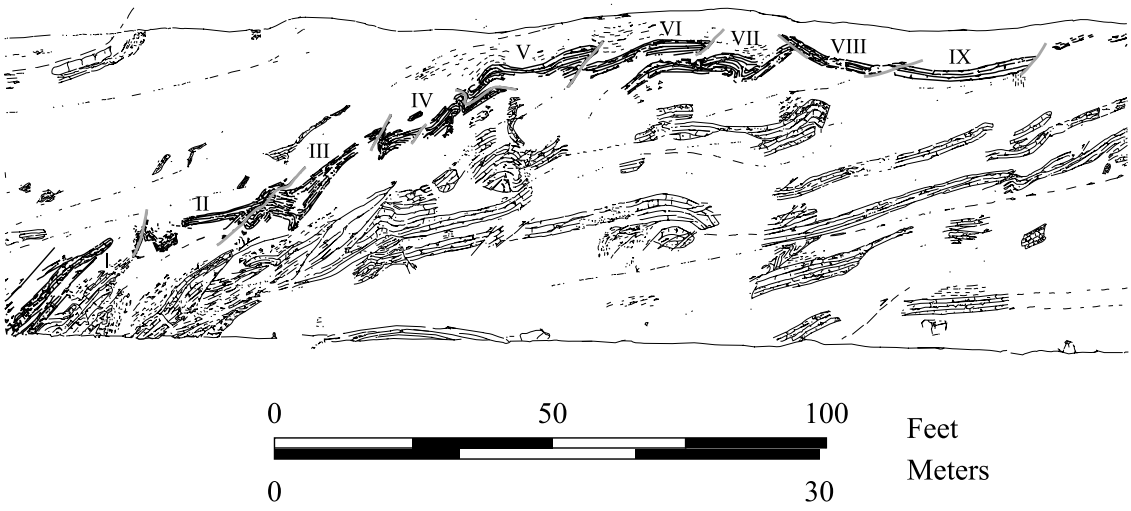

Fig. 2. Cross-section of Sun River outcrop (after Johnson, 1988). Non-dimensional wavelength measurements were made at several places in the topmost layer (see roman numerals). Folds typically range from three to four, with thrust slices around seven.

Given the close association of these features in this single outcrop, we believe it is reasonable to interpret them as all arising from shortening along the layer. Our observations and measurements show that in some examples the fault formed first, but in others the folds formed first. Still in others both the folds and faults occur in complexes, from which we infer that they formed during the same interval of deformation. The non-dimensional wavelengths for thrust slices tend to be about seven, whether or not the associated sandstone unit is folded. Also, non-dimensional wavelengths for folds are generally less than seven, ranging as low as about three. Since the exposure of the sandstone layers is varied and the layers in places are thickened due to small-scale wedging, it is not meaningful to be more precise. The sheared limb folds are interpreted to be precursors to faulting, rather than due to fault 'drag'. While some small-scale ramping occurs within individual units of the sandstone layers creating small, ramp–fold wedges, the overall style cannot be classified simply as either ramp folding or as fault propagation folding.

The foregoing observations suggest that the sandstone units in this outcrop were in a mechanically transitional state during shortening, where both 'distributed' and 'localized' modes of deformation were possible. Consequently, any model for this style of deformation must incorporate, in addition to a more competent layer within a less competent matrix, a mechanism which results in the formation of both folds and faults under layer parallel shortening.

3. Layer parallel shortening of stratified viscoelastic media

In this section the derivation of key results in the theory of nonlinear viscoelastic deformation and a rationale for using the second order fluid (SOF) equation (Coleman and Noll, 1960) are presented. Mathematical details are included within Appendix A. Superscript asterisks (*) are used throughout to denote dimensional quantities. From the outset deformation is assumed to be incompressible, isothermal and inertialess, in order to make the analysis tractable. In general the success of simple models, like this one, can provide physical insight into otherwise complex phenomena and boost confidence in the modeling approach, while sacrificing quantitative rigor. It is hoped that the reader will gain some of the former from this work, while forgiving the latter. Readers interested in learning more about these methods should consult continuum mechanics texts (e.g. Segel, 1987; Lin and Segel, 1994) and the cited literature.

Consider the two-dimensional deformation of a single layer of thickness H^*, composed of relatively competent material in no-slip contact with two semi-infinite half-spaces of less competent material (Fig. 3). A coordinate system (x, z) is chosen such that the x-axis lies at the mean position of the layer, with the z-axis perpendicular to the layer. The layer is subjected to steady layer-parallel shortening in pure shear. This is achieved by assuming a basic velocity distribution which is proportional to distance from the origin and scaled to an assumed far field dimensional velocity V^*, such that the deformation is shortening in the x-direction and extending in the z-direction. Deformation is assumed to be incompressible, thereby simplifying the mass conservation equation (A1). It is also assumed to be isothermal, allowing further simplification by neglect of the heat equation, and so slow that inertial terms can be neglected in the momentum balance equation (A2). Finally, we assume that the deforming media are SOFs, with constitutive equation (1), which is expanded upon in Appendix A:

$$T^* = \eta^* A_1^* + \beta^* A_1^{2*} + \gamma^* A_2^*. \tag{1}$$

We use the SOF to model rock rheological behavior

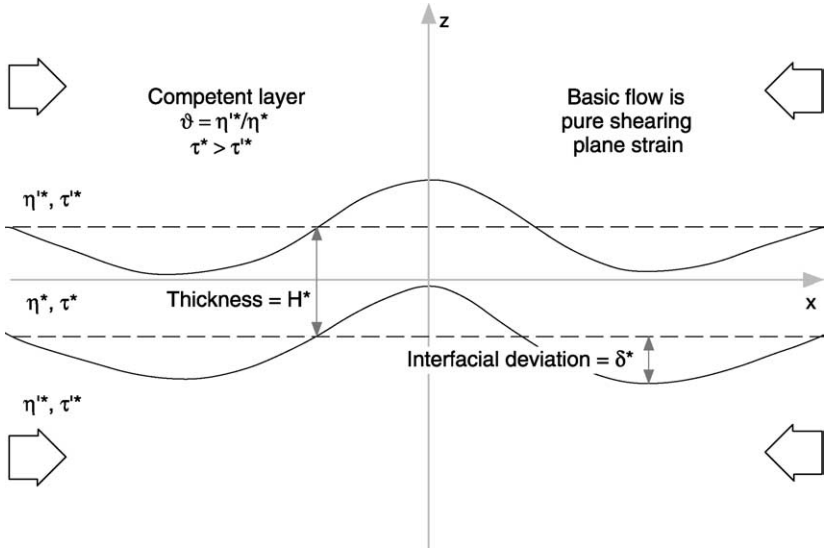

Fig. 3. Assumed model geometry depicting folding of a single competent layer in layer parallel compression.

because it is the simplest nonlinear constitutive equation exhibiting viscoelastic effects (Rundle and Passman, 1982). The SOF includes both linear and nonlinear viscosity fluids (including power law fluids) as special cases (Joseph, 1989), and therefore provides a consistent basis for comparing results of extant analytical theories (Biot, 1961; Ramberg, 1963; Chapple, 1968; Sherwin and Chapple, 1968; Fletcher, 1974, 1995; Smith, 1975, 1977, 1979; Alexander and Watkinson, 1989; Goff et al., 1996; Patton, 1997), recent numerical simulations (Zhang et al., 1996; Hobbs et al., 2000; Schmalholz and Podladchikov, 2000; Muhlhaus et al., 2002), and our own work. However, it is implausible that power law representations of rock mechanics data are directly applicable to deformations in deep time (Paterson, 1987; Rutter and Brodie, 1991). Linear viscoelasticity (e.g. Maxwell rheology) is also problematic, notably in the prediction of excessive compressive strengths for rocks and the need to impose localization mechanisms to achieve realistic deformation (e.g. McAdoo and Sandwell, 1985). Localization in real rocks arises self-consistently based on rock fabric, grain size distribution, fluid and thermal diffusive processes, etc. under applied forcing and therefore by definition is 'nonlinear', but as a function of what? For these reasons we sought a nonlinear constitutive equation suited to the study of slow deformation, which incorporated viscoelasticity, finding it in the SOF. This equation has been used to study simple shearing deformation (Hobbs, 1972), rock mechanics data (Passman, 1982), melts and magmatic suspensions (Spera et al., 1988), transverse oceanic ridges (Bercovici et al., 1992), and the formation of lithospheric plates (Patton et al., 2000).

We scale and non-dimensionalize the model system, the purpose of which is to expose the physics and simplify subsequent analysis. At any time this step can be undone by introducing measured or assumed values of the dimensional quantities appearing in the problem. Prior to this, however, we take a closer look at the dimensions of the coefficients appearing in the SOF (Eq. (1)). Dimensional analysis (Lin and Segel, 1994) is a simple yet subtle tool of applied mathematics. Use of this procedure in Eq. (1) shows that the first and second normal stress coefficients γ^* and β^* have dimensions (mass/length). Given that shear viscosity η^* has dimensions (mass/length–time), γ^* and β^* can be represented by the product of η^* and 'natural' times for the first and second normal stress differences arising as a function of deformation history (Truesdell, 1964). The former time, identified as τ^*, is the 'relaxation time' common to all viscoelastic theories, while the latter one is associated with nonlinear viscosity (e.g. power law) effects. Consequently, it is assumed that $\gamma^* = -\tau^*\eta^*$, where the negative sign on τ^* is necessary to make the last two terms of Eq. (A3c) additive in the stress equation (A3a). The first two terms of Eq. (A3c) are neglected because they are explicitly time dependent and thereby contradict the assumed steady deformation. Furthermore nonlinear viscosity effects are neglected in this simplified analysis and are well documented elsewhere (e.g. Fletcher, 1974, 1995; Smith, 1977, 1979). Consequently we define $\beta^* = 0$ throughout the balance of the paper.

In the folding of viscous layers competence contrast is naturally expressed as a viscosity ratio, here defined as $\vartheta = \eta'^*/\eta^*$ (Fig. 3). However, while viscosity contrasts are possible in viscoelastic folding, they will be shown to be of secondary importance to localization processes. Competence contrast can also be defined on the basis of relaxation time, τ_*, hence we assume that $\tau^* > \tau'^*$. Note that in SOFs the shear viscosity scales the magnitude of stress (Eq. (A4c)), a property found earlier to be relevant in the plate formation problem of geodynamics (Patton et al., 2000).

Scaling all dimensional lengths, times, and stresses by competent layer thickness (H^*), inverse strain rate (H^*/V^*), and shear stress ($\eta^* V^*/H^*$), respectively, and introducing

appropriately scaled variables into the model system (Eqs. (A1), (A2) and (A3a)–(A3c)) leads to the non-dimensional system of equations (A4a)–(A4c). Observe that dimensional quantities like shear viscosity and relaxation time previously found throughout the model system are now found only in the two dimensionless parameters ϑ and Wi. ϑ is the viscosity contrast defined earlier while Wi is the Weissenberg number, defined as a ratio of time scales, $Wi=\tau^*/(H^*/V^*)$.

Substituting the stress equation (A4c) into the momentum balance equation (A4b) and writing everything in partial derivatives leads to Eqs. (A5a)–(A5c). Eqs. (A5a)–(A5c) can be manipulated producing a differential operator on the stream function (Patton, unpublished notes). However, solving for the stream function in this case requires numerical methods. Because the purpose of this paper is to gain insight into the mechanics of the assumed rheology and how it might relate to rock deformation, we shall focus on a purely analytical means of solution. Numerical simulations based on this formulation are work in progress.

A method commonly used in folding theories to further simplify the problem is linearization of the flow field. This is most often achieved by expanding the flow in series based on a small dimensionless parameter, defined by the deviation of the layer interfaces from an initially assumed plane condition. Here interfacial deviation δ^* (Fig. 3) is scaled by layer thickness so that the small parameter $\varepsilon=\delta^*/H^*$. In the expansion equations (A6a)–(A6c) ε is assumed to be finite but much smaller than unity ($0<\varepsilon\ll 1$). This procedure strictly limits the validity of the mathematical formulation to infinitesimal amplitude, or low limb dip folding. Finite amplitude effects are certainly important to fold growth, particularly in studies of fold shape. However, linearization in this case reduces the complexity of the problem while retaining terms proportional to Wi, consistent with the goal of this paper. Terms proportional to ε in Eqs. (A6a)–(A6c) are commonly referred to as perturbations, because they represent small deviations from the assumed basic flow state. In this case the basic flow is assumed to be a pure shearing plane strain that satisfies Eqs. (A5a)–(A5c) identically. Consequently, all terms containing the basic flow drop out of the analysis, leaving only the perturbation flow. Substituting Eqs. (A6a)–(A6c) into Eqs. (A5a)–(A5c), canceling a factor ε common to all terms, and neglecting all remaining terms proportional to ε produces Eqs. (A7a)–(A7c). Observe, for example, that where before there were 11 terms proportional to Wi in Eq. (A5b), there are now only three in Eq. (A7b).

Eqs. (A7a)–(A7c) are relatively easy to write in closed form using a dimensionless stream function $\psi(x, z)$, where $u_1=\partial\psi/\partial z$ and $w_1=-\partial\psi/\partial x$. This technique is motivated by the incompressibility equation (A7a), which the stream function satisfies identically (Batchelor, 1967). Substituting for the velocity components in terms of the stream function and combining the expressions (A7b) and (A7c) leads to the partial differential equation (2) governing perturbation flow:

$$\alpha^2\frac{\partial^4\psi}{\partial x^4}+\left(1+\alpha^2\right)\frac{\partial^4\psi}{\partial x^2\partial z^2}+\frac{\partial^4\psi}{\partial z^4}=0 \tag{2}$$

where

$$\alpha^2=\frac{1-2Wi}{1+2Wi}. \tag{3}$$

Due to our earlier assumption on γ^* in Eq. (1) the relative viscosity ϑ does not appear in Eq. (2).

Low amplitude deviations of the folding layer from an initially assumed planar state (Fig. 3) can be analyzed using separable normal mode solutions (Eq. (A10)). Substituting Eq. (A10) into Eq. (2) leads to the characteristic equation:

$$r^4-\left(1+\alpha^2\right)r^2\omega^2+\alpha^2\omega^4=0 \tag{4}$$

with roots

$$r=\pm\omega_1 \quad \text{or} \quad r=\pm\alpha\omega_2. \tag{5}$$

The general solution of Eq. (2) is therefore dependent on Wi. This can be visualized by plotting $|\alpha|$ versus Wi (Fig. 4), revealing dissimilar deformation regimes. For (I) $0<Wi<$ ½, (II) $Wi=$½, and (III) ½$<Wi<\infty$, the general solution is given by Eqs. (A13a)–(A13c), respectively. Patton (1997) used the regime I solution to model folding, as will be discussed in Section 5.

Clearly Eq. (2) is singular as $Wi\to$½ (i.e. $\alpha\to 0$). Singularities like this one are commonly associated with dramatic changes in physical behavior. Because Wi has specific physical meaning, this implies a change in the character of deformation when the relaxation time exceeds $H^*/2V^*$. For example, for a meter thick competent bed deformed at a tectonic plate velocity of about 10^{-8} m/s this threshold relaxation time is about 10^7 s ($\sim$1 year) (Eq. (A14)). But what does $|\alpha|$ represent physically? It can be shown using a change of variables that $|\alpha|$ uniquely and naturally scales lengths in this region of dramatic change (see Section 9.2 of Lin and Segel (1994) and Eq. (A17)).

In the initial statement of the folding problem we assumed incompressibility and neglected inertial terms. We also retained two normal stress terms, heretofore neglected in folding analyses, which appear in Eq. (A3c). The singular behavior of Eq. (2) is linked to these terms. Physically, this implies that at some critical value of viscoelastic strain energy the character of deformation can change, presumably from distributed to localized, and possibly inertial, modes (Fig. 4). Thus $|\alpha|$ must be inversely proportional to strain energy in the deforming medium, so that strain energy is high when $|\alpha|$ is small. As such $|\alpha|$ appears to modulate the stability of the resulting perturbation motions. For these reasons we call it the 'spectral radius', consistent with that term's use in analyzing the stability of finite difference methods.

At this point it is useful to recall the reciprocal relationship between wavenumber ω and length ℓ, that is

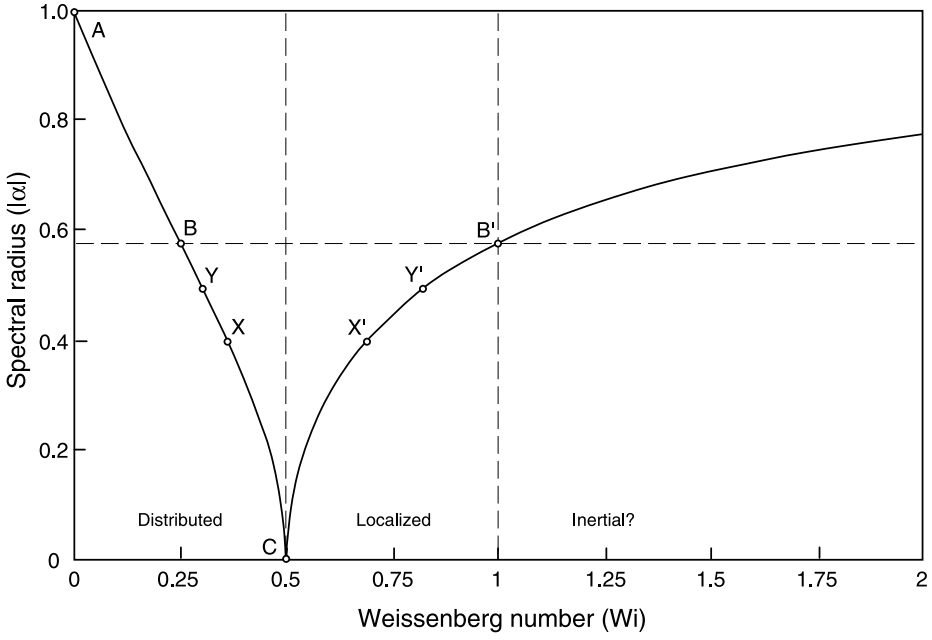

Fig. 4. Plot of spectral radius (Eq. (3)) versus Weissenberg number, *Wi*. This plot reveals at least three dissimilar regimes for the deformation of nonlinear viscoelastic media.

$\ell \propto \omega^{-1}$. Immediately, we see that the roots (Eq. (5)) predict the existence of two independent length scales, in contrast to the linear viscous and elastic models, which predict only one. In order to distinguish between such linear ('biharmonic') models and the nonlinear viscoelastic model presented here, we call Eq. (2) the 'diharmonic' equation. In the balance of this paper the ratio of these length scales is identified with observed non-dimensional wavelengths of folds and thrust faults.

Quite independent of their physical interpretation, further analysis of the roots (Eq. (5)) leads to a scaling relationship. First, we write $\ell_1 \sim \omega_1^{-1}$ and $\ell_2 \sim (\alpha\omega_2)^{-1}$ and form the ratio $\ell_2/\ell_1 \sim (\alpha\omega_2/\omega_1)^{-1}$. Now consider that although *Wi* is defined as a ratio of time scales $\tau^*/(H^*/V^*)$, where τ^* is relaxation time and H^*/V^* is the reciprocal of the imposed basic strain rate, it could just as easily be written as a ratio of length scales $(\tau^* V^*)/H^*$. This duality of space and time is a generally recognized property of diffusive systems (Turcotte and Schubert, 2002, p. 149). Consequently, we are free to identify *Wi* as the non-dimensional wavenumber appearing in the scaling relationship derived above; that is $Wi \equiv \omega_2/\omega_1$. Although this choice is by no means unique, it is a most convenient one given the overall context of the problem. As a result, we can redefine the scaling relationship as:

$$\mathsf{L} \sim \left(|\alpha| Wi\right)^{-1}. \tag{6}$$

Observe in Eq. (6) that $|\alpha|$ appears in the denominator, consistent with the inverse relationship between strain energy and $|\alpha|$ deduced above in connection with the singular behavior of Eq. (2). Consequently we shall refer to L generically as the 'scalar energy density' (Fig. 5).

4. Viscoelastic strain energy principle

A useful starting point for interpreting Eq. (6) is to imagine an experiment in which a cylindrical rock specimen is subjected to progressive end loading. For relatively small strains the work done on the cylinder is, to a first approximation, stored as energy throughout the specimen. As the load is increased the additional work done on the cylinder eventually results in localization of deformation and rupture. Traditionally such experiments have been interpreted in terms of Mohr–Coulomb failure surfaces in stress space, an interpretation that underpins much of the engineering strength of materials theory. Of course this is a reasonable description of short-term behavior, but does not address the issue of the longer time scales assumed to exist in natural rock deformation.

The scalar energy density (Eq. (6)) is defined in terms of two factors having different qualities. Recall that *Wi* can act as both a non-dimensional time scale and a non-dimensional wavenumber. In the former role it has an intrinsic quality related to the history of deformation. Through Eq. (3), the spectral radius $|\alpha|$ takes on unique values (real, zero, or imaginary) depending on *Wi*, and by association also has an essentially intrinsic quality. Therefore we define the *intrinsic energy density* as $\mathsf{L}_\mathrm{I} \sim |\alpha|^{-1}$ (Fig. 5), and interpret it as the internal energy state of a material particle resulting from the integrated history of motions around the particle, beginning in the far field. Observe that L_I grows large as $Wi \to ½$ emphasizing the transitional nature of the model at that value of *Wi*.

In its wavenumber role *Wi* has an extrinsic quality related to non-dimensional wavelengths of the deforming

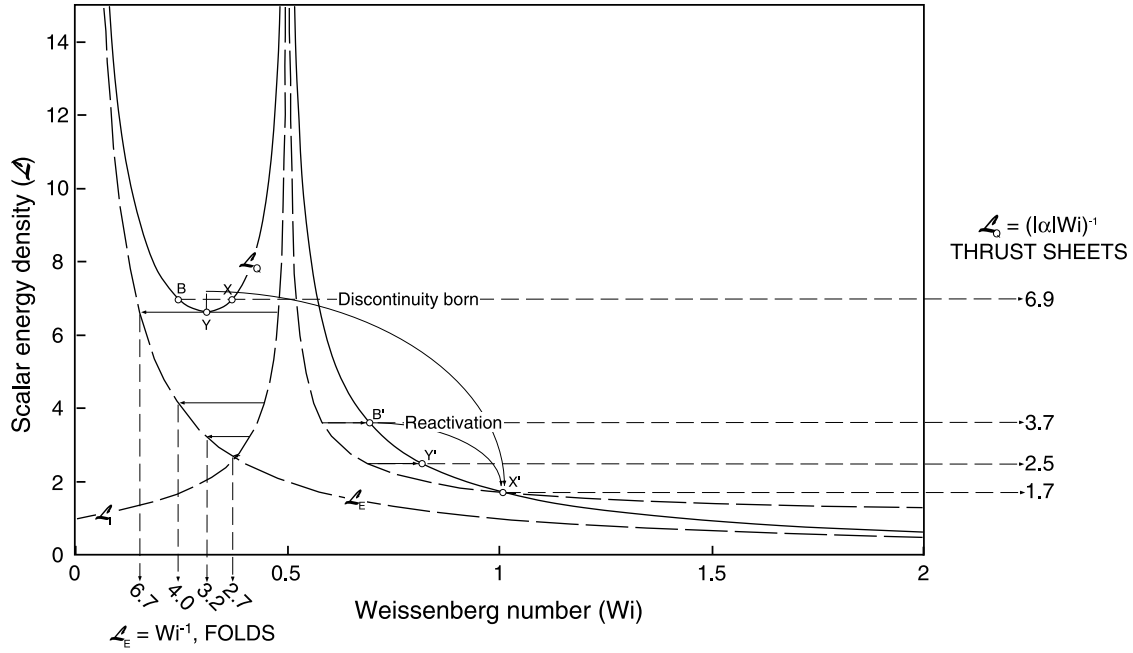

Fig. 5. Plot of scalar energy density versus wavenumber, *Wi*. L_I, L_E, and L_Q denote the intrinsic, extrinsic, and quasi-static energy densities, respectively. The distributed-localized transition (B–X→X′) occurs when L_I exceeds a value of about seven at the bottom of the energy well (Y).

competent layer (Fig. 3). Such deformation is necessarily 'distributed'. Thus we define the *extrinsic energy density*, $L_E \sim Wi^{-1}$ (Fig. 5), and interpret it as the energy threshold for the onset of distributed deformation—in this case folding. This is equivalent to folding being a specific mode of stress relaxation, which is energetically possible only at finite strain rate. Horizontal 'tie' lines, drawn parallel to the wavenumber axis from the intrinsic to the extrinsic energy densities (Fig. 5), provide a ready means of identifying the associated range of non-dimensional fold wavelengths. Extending the rock cylinder analogy a bit further, it is reasonable to assume that at some point the 'strength' of the material particle will be exceeded, resulting in localized failure—a discontinuity 'born'. It is desirable, then, within the context of present theory to define an energy threshold that governs this transition from distributed to localized deformation. Such a threshold is in fact provided by Eq. (6), because $|\alpha|$ appears in the denominator of that expression. Because of the assumed 'slow flow' approximation we call this energy threshold the *quasi-static energy density*, $L_Q \sim (|\alpha| Wi)^{-1}$ (Fig. 5). This is equivalent to faulting being a specific mode of stress relaxation, which is energetically possible only at relatively high levels of intrinsic energy. Other likely modes of relaxation or energy dissipation include cataclasis and heat production. Once the transient motions associated with faulting cease, forcing starting in the far field can begin anew, perhaps leading to reactivation of the discontinuity. In engineering strength of materials theory the distributed–localized transition (B–X→X′) would be called cohesive failure, while reactivated slip (B′→X′) would be called frictional failure. Horizontal tie lines, now drawn from the intrinsic to the quasi-static energy densities, provide a means of identifying the non-dimensional wavelengths associated with new and reactivated faults.

Obvious implications of the preceding discussion are that distributed deformation is quite likely for normalized wavelengths greater than about 2.7, and that all localized failures are preceded by some degree of distributed deformation. Here is theoretical support for the fold-first hypothesis. The maximum wavelength of distributed deformation in the layer is about 6.7, i.e. its tie line is tangent to L_Q at Y. Observe that L_Q exhibits an energy 'well' centered at about $Wi = 0.3$, in which L_Q takes values of about 6.7–6.9. The implication here is that distributed deformation will spontaneously 'yield' to localized failure if L_I exceeds values of about 7. Formation of a new discontinuity in this manner can be thought of as a constitutive instability, depending more on the local history of deformation than the degree of far field forcing. Once such a discontinuity exists it can be reactivated at energy levels well below the critical value (i.e. 3.7 or less). Finally, recall that L_I rapidly grows as $Wi \rightarrow ½$. In the context of the rock cylinder experiment, we note that this implies that ultimate material strength is best measured in specimens two times longer than they are wide. This prediction is consistent with current ASTM standard and practical experience.

5. Viscosity contrasts, numerical simulations, and Deborah number

It is interesting to compare the results of the preceding

section with those from earlier folding work in which a viscosity contrast was explicitly included (Fig. 6). We note that the frequency distribution of non-dimensional wavelengths for natural folds ranges from about 3 to 35, with modes in the range 4–7 (Sherwin and Chapple, 1968). These observations are difficult to reconcile with dominant wavelength theory which suggests that the mode of the distribution should approximate the Biot–Ramberg wavelength for competence contrasts greater than about 100, i.e. non-dimensional wavelengths greater than about 15 (Biot, 1961; Ramberg, 1963). This problem also pertains to dominant wavelength numerical computations using Maxwell elastic–viscous and elastic–plastic composite rheologies (Zhang et al., 1996). Sherwin and Chapple (1968) explained this discrepancy for the viscous case by allowing for significant layer parallel shortening at competence contrasts ranging from about 14 to 30. Observe that Zhang et al.'s (1996) composite rheologies are indistinguishable from the viscous case in dominant wavelength theories for competence contrasts less than about 50. Using the general solution (A13a), Patton (1997) found that residual normal stresses destabilize folds at wavelengths less than the so-called 'transition wavelength', while stabilizing those at longer wavelengths. Clearly it is possible to reconcile fold observations with this latter viscoelastic theory at competence contrasts of about 10–36, consistent with those found by Sherwin and Chapple (Watkinson and Patton, 2001).

Recent numerical studies of finite amplitude folding in Maxwell viscoelastic media have shown the simultaneous development of two fold wavelengths (Schmalholz and Podladchikov, 2000; Muhlhaus et al., 2002). Schmalholz and Podladchikov (2000) assert that while the Deborah number, *De*, has little effect on this type of folding their new '*R*' parameter has a significant one. Note that *De* and *Wi* are often used interchangeably in the literature (Larson, 1992). However, using definitions provided in their paper it can be shown that so-called 'viscoelastic mode' folding has growth rates equal to $4De^{1/2}/3\vartheta$ and dominant wavelengths equal to $\pi De^{-1/2}$. Note that '*R*' appears in neither of these expressions. Furthermore, while the growth rate's dependence on *De* is indeed weak, consistent with their assertion, its dependence on viscosity contrast is rather strong, $1/\vartheta$ instead of $(1/\vartheta)^{2/3}$. Consequently, it appears that their results are dominated by the effects of viscosity contrast, rather than viscoelasticity. Also note that their dominant wavelength, although independent of viscosity contrast, is proportional to $De^{-1/2}$ rather than De^{-1} as suggested by the viscoelastic strain energy principle (Eq. (6)).

Muhlhaus et al. (2002) report that the characteristic length scale of emerging fold patterns in their model tends to zero with increasing relaxation time, although the specific proportionality is not stated. They also mention numerical difficulties such as mesh sensitivity arising at high elasticities, and show how couple stresses can be used to stabilize short wavelength folds. Finally, they suggest that large couple stresses, if included in such models, could lead to failure of the bending rock layer producing a discontinuity. These qualitative findings are broadly consistent with those discussed above in connection with Eq. (6). Consequently, we predict that failure should occur in simulations incorporating couple stresses at $De \sim ½$.

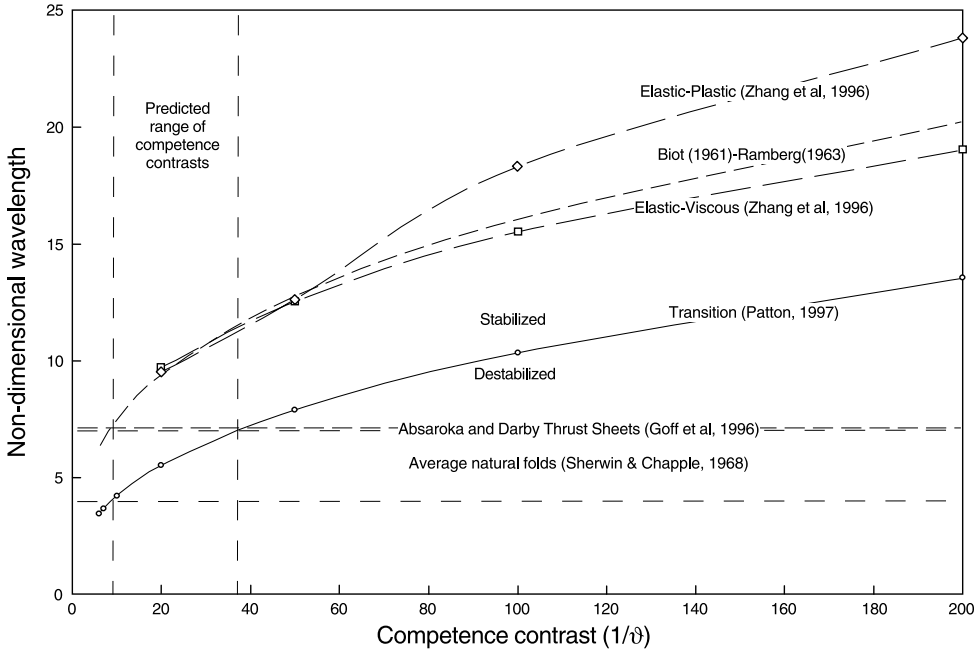

Fig. 6. Plot of non-dimensional wavelength versus competence contrast showing relationship between observational data and various folding theories (after Watkinson and Patton, 2001).

6. Observations across a range of scales

In this section we summarize and discuss observations from published studies spanning a range of scales, from microscopic splay cracks in ice to lithospheric scale folds. The discussion is thematic and really addresses the data more than the models used to interpret it. The studies summarized here are but a few of those we have found which appear to express the viscoelastic energy principle.

The fold first hypothesis holds that early-formed folds serve to localize thrust ramps in layered sedimentary rock sequences. In testing this idea Goff et al. (1996) present measurements of thrust sheet length to thickness ratios for two thrust sheets of the Sevier fold–thrust belt, Wyoming. These observations are at a larger scale than our own at Sun River, and are constrained by seismic and drill hole data. The non-dimensional thrust sheet lengths they report are 7.05 ± 0.26 and 7.15 ± 0.87 for the Absaroka and Darby thrust sheets, respectively. These values are identical, within reported uncertainties, to the critical non-dimensional wavelength of about 6.9 predicted by Eq. (6) for localization of deformation.

A body of work dating from the 1980s makes clear large-scale deformation of the oceanic lithosphere in the central Indian Basin. McAdoo and Sandwell (1985) present geophysical observations, including Seasat altimeter data, which suggest lithospheric scale folding with dimensional wavelengths ranging from about 130 to 250 km. The highest number of geoid undulations occurs at about 190 km. They also present a model, based on the Goetz–Evans yield strength envelope, to explain this range of wavelengths while avoiding the unrealistically high stresses associated with Euler buckling. McAdoo and Sandwell (1985) estimate the average thickness of the lithosphere involved in the folding to be about 46 km, based on the half-space cooling model (Parsons and Sclater, 1977). Thus, the equivalent range of normalized wavelengths is about 2.8–5.4, with a maximum at about 4. These values are broadly consistent with the distributed modes predicted by the present theory. It is interesting to note that the Seasat observations have a bimodal distribution (McAdoo and Sandwell, 1985, their fig. 7), with maxima at about 190 and 290 km. Furthermore, the overall range of dimensional wavelengths appears to be 75–325 km (i.e. non-dimensional wavelengths from 1.6 to 7.1). We speculate that this might indicate the presence of both folds and thrust faults of the lithosphere.

Interest in the central Indian Basin deformation prompted laboratory model analog work as well. Bull et al. (1992) conducted a series of layered analog experiments, properly scaled to geologic conditions, to test the preferred mode of deformation. Based on results from power law fluid theory, there was some controversy about whether the lithosphere would shorten by folding or pinch and swell. Their experiments showed that the model lithosphere folded at an average value of about 6.9. They also mention that faults formed in their models, following the appearance of folds. These observations are in excellent agreement with the present theory, which therefore explains their heretofore 'poorly understood' association.

Up to this point all of the observations discussed have been at intermediate to large scale. We shall finish this discussion by looking briefly at the opposite extreme. Schulson et al. (1999) describe compression experiments on 2D microstructural (S2 columnar) ice, in which they observed 'splay cracks' forming adjacent to tensile wing cracks near sliding grain boundaries. The splay cracks formed only on one side of the sliding boundary, and ultimately were the locus of shear faulting in the specimens. Prior to localized failure splay cracks were observed to form throughout the specimens, wherever sliding parent cracks occurred. Based on these observations the authors argued that splay cracks play a crucial role in localizing failure, specifically by producing a series of microcolumns which first bend and then finally break. Load shed from column to column ultimately leads to a dynamic shear failure. Significantly, Schulson et al. (1999) report 'slenderness' (length/width) ratios for these microcolumns of 3.1–7.2. These values apparently pertain to intact (i.e. pre-localization) microcolumns from step strain experiments, where the macroscopic specimen is still intact and the peak (failure) stress is not yet reached. These observations are in excellent agreement with the range of non-dimensional wavelengths predicted by our viscoelastic strain energy principle, for both distributed and localized deformations. This finding thus lends theoretical support to Schulson et al.'s (1999) assertion that splay microcolumn failure provides a critical localization mechanism in brittle solids.

7. Conclusion

The strength of the approach described in this paper is the explicit demonstration of a transition from distributed to localized modes of deformation, specifically as expressed in the folding and thrust faulting of a competent rock layer. This is amply supported by the agreement between observations at Sun River, and elsewhere, and the predictions of the strain energy principle (i.e. distributed and localized modes scaling as $L_E \sim Wi^{-1}$ and $L_Q \sim (|\alpha| Wi)^{-1}$, respectively). The analysis presented here, although simplified, raises numerous questions that serve as an outline for future research in structural geology, geodynamics, rock mechanics, and seismology. Furthermore, the insights arising from this analysis provide motivation to reconsider both empirical and observational data at many spatial and temporal scales.

Acknowledgements

Thanks to Ray Fletcher and Bruce Hobbs for their

insightful reviews. Special thanks to Dr Hobbs for his unqualified support for this work.

Appendix A. Derivation of the 'diharmonic' equation governing deformation of nonlinear viscoelastic materials

The field equations for incompressibility (Eq. (A1)) and momentum balance (Eq. (A2)) in an isothermal, inertialess continuum, in the absence of body forces, are assumed to be valid:

$$0 = \nabla^* \cdot v^* \tag{A1}$$

$$0 = -\nabla^* p^* + \nabla^* \cdot T^* \tag{A2}$$

with velocity v^*, pressure p^*, and differential stress T^* defined by the second order fluid equation (A3a) (Coleman and Noll, 1960):

$$T^* = \eta^* A_1^* + \beta^* A_1^{2*} + \gamma^* A_2^* \tag{A3a}$$

where

$$A_1^* = \nabla^* v^* + (\nabla^* v^*)^{\mathrm{T}} \tag{A3b}$$

and

$$A_2^* = \frac{\partial A_1^*}{\partial t^*} + \left(v^* \cdot \nabla^*\right) A_1^* - (\nabla^* v^*)^{\mathrm{T}} A_1^* - A_1^* \nabla^* v^*. \tag{A3c}$$

The superscript * is used to identify dimensional quantities. A_1^* (Eq. (A3b)) and A_2^* (Eq. (A3c)) are the first and second kinematic tensors, respectively (Rivlin and Ericksen, 1955), and note that A_2^* has been expanded as an upper convected derivative (Oldroyd, 1950; Larson, 1992). $()^{\mathrm{T}}$ denotes the transpose of a tensor and t^* denotes time. The coefficients η^*, γ^*, and β^* denote shear viscosity, and the first and second normal stress coefficients, respectively. Observe that $A_1^* = 2D^*$, where D^* is the usual rate of deformation tensor.

Consequently, if $\gamma^* = \beta^* = 0$, then the formulation reduces to that for a Newtonian fluid. Also, if only $\gamma^* = 0$, then the formulation is that for a nonlinear viscous (i.e. Reiner–Rivlin) fluid. Power law fluids are a special case of the latter fluid. In what follows we assume that β^* is identically zero and that $\gamma^* = -\eta^* \tau^*$, where τ^* is relaxation time.

Scaling length, time, and stress by competent layer thickness (H^*), inverse strain rate (H^*/V^*), and shear stress ($\eta^* V^*/H^*$), respectively, and introducing appropriately scaled variables into Eqs. (A1), (A2) and (A3a)–(A3c) leads to the following system of equations:

$$0 = \nabla \cdot v \tag{A4a}$$

$$0 = -\nabla p + \nabla \cdot T \tag{A4b}$$

$$T = 2\vartheta D + 2\vartheta Wi\left[(\nabla v)^{\mathrm{T}} D + D(\nabla v)\right] \tag{A4c}$$

where $\vartheta = \eta^*/\eta_0^*$ and $Wi = \tau^* V^*/H^*$.

The non-dimensional parameters ϑ and Wi are the relative viscosity and Weissenberg number, respectively. Substituting the constitutive equation (A4c) into the momentum balance equation (A4b) and expressing everything in partial derivatives leads to the following equations:

$$0 = \frac{\partial u}{\partial x} + \frac{\partial w}{\partial z} \tag{A5a}$$

$$\begin{aligned} 0 = {} & -\frac{\partial p}{\partial x} + \vartheta \nabla^2 u + \vartheta Wi\left[8\frac{\partial u}{\partial x}\frac{\partial^2 u}{\partial x^2}\right. \\ & + 4\left(\frac{\partial u}{\partial z} + \frac{\partial w}{\partial x}\right)\frac{\partial^2 u}{\partial x \partial z} + 2\frac{\partial u}{\partial z}\nabla^2 w \\ & + \left(\frac{\partial u}{\partial z} + \frac{\partial w}{\partial x}\right)\left(\frac{\partial^2 u}{\partial x \partial z} + \frac{\partial^2 w}{\partial z^2}\right) \\ & \left. + 2\left(\frac{\partial w}{\partial z}\frac{\partial^2 u}{\partial z^2} + \frac{\partial u}{\partial x}\frac{\partial^2 w}{\partial x \partial z}\right)\right] \end{aligned} \tag{A5b}$$

$$\begin{aligned} 0 = {} & -\frac{\partial p}{\partial z} + \vartheta \nabla^2 w + \vartheta Wi\left[8\frac{\partial w}{\partial z}\frac{\partial^2 w}{\partial z^2}\right. \\ & + 4\left(\frac{\partial u}{\partial z} + \frac{\partial w}{\partial x}\right)\frac{\partial^2 w}{\partial x \partial z} + 2\frac{\partial w}{\partial x}\nabla^2 u \\ & + \left(\frac{\partial u}{\partial z} + \frac{\partial w}{\partial x}\right)\left(\frac{\partial^2 u}{\partial x^2} + \frac{\partial^2 w}{\partial x \partial z}\right) \\ & \left. + 2\left(\frac{\partial u}{\partial x}\frac{\partial^2 w}{\partial x^2} + \frac{\partial w}{\partial z}\frac{\partial^2 u}{\partial x \partial z}\right)\right] \end{aligned} \tag{A5c}$$

Further simplification of the problem, still retaining terms proportional to Wi, can be achieved by linearizing the solution around a pure shearing basic flow. Assuming a basic flow $(u_0, w_0) = (-x, z)$ and introducing the small parameter $\varepsilon = \delta^*/H^*$, where δ^* is the amplitude of growing fold-like disturbances at the layer interfaces (Fig. 3), Eqs. (A5a)–(A5c) can be transformed using solutions of the following form:

$$u(x, z, t) = u_0(x) + \varepsilon u_1(x, z, t) + O\left(\varepsilon^2\right) \tag{A6a}$$

$$w(x, z, t) = w_0(x) + \varepsilon w_1(x, z, t) + O\left(\varepsilon^2\right) \tag{A6b}$$

$$p(x, z, t) = p_0(x) + \varepsilon p_1(x, z, t) + O\left(\varepsilon^2\right) \tag{A6c}$$

Upon substituting Eqs. (A6a)–(A6c) into Eqs. (A5a)–(A5c), canceling the common factor ε, and neglecting terms $O(\varepsilon)$ and higher, we obtain Eqs. (A7a)–(A7c). Observe that the basic flow (u_0, w_0) vanishes entirely because it satisfies Eqs. (A5a)–(A5c) identically, leaving only the linearized flow (u_1, w_1):

$$0 = \frac{\partial u_1}{\partial x} + \frac{\partial w_1}{\partial z} \tag{A7a}$$

$$0 = -\frac{\partial p_1}{\partial x} + \vartheta \nabla^2 u_1 + \vartheta Wi\left[-8\frac{\partial^2 u_1}{\partial x^2} + 2\frac{\partial^2 u_1}{\partial z^2} - 2\frac{\partial^2 w_1}{\partial x \partial z}\right] \tag{A7b}$$

$$0 = -\frac{\partial p_1}{\partial z} + \vartheta \nabla^2 w_1 + \vartheta Wi\left[8\frac{\partial^2 w_1}{\partial z^2} - 2\frac{\partial^2 w_1}{\partial x^2} + 2\frac{\partial^2 u_1}{\partial x \partial z}\right] \tag{A7c}$$

These equations can be solved in closed form using a dimensionless stream function $\psi(x, z)$, where $u_1 = \partial\psi/\partial z$ and $w_1 = -\partial\psi/\partial x$, which satisfies the incompressibility equation (A7a) identically. Substituting for the velocity components in terms of the stream function and combining the resulting expressions leads to the 'diharmonic' equation:

$$\alpha^2 \frac{\partial^4 \psi}{\partial x^4} + \left(1 + \alpha^2\right) \frac{\partial^4 \psi}{\partial x^2 \partial z^2} + \frac{\partial^4 \psi}{\partial z^4} = 0 \tag{A8}$$

where

$$\alpha^2 = \frac{1 - 2Wi}{1 + 2Wi}. \tag{A9}$$

Because folds in this model are of infinitesimal amplitude, $0 < \varepsilon \ll 1$, they can be analyzed using separable normal mode solutions of the form:

$$\psi = \mathrm{e}^{\mathrm{i}\omega x + rz} \tag{A10}$$

Substituting Eq. (A10) into Eq. (A8) leads to the characteristic equation:

$$r^4 - \left(1 + \alpha^2\right) r^2 \omega^2 + \alpha^2 \omega^4 = 0 \tag{A11}$$

with roots

$$r = \pm\omega_1 \quad \text{or} \quad r = \pm\alpha\omega_2. \tag{A12}$$

The general solution of Eq. (A8) is therefore dependent on Wi. For (I) $0 < Wi < ½$, (II) $Wi = ½$, and (III) $½ < Wi < \infty$, the general solution is given by Eqs. (A13a)–(A13c), respectively. Patton (1997) used the regime I solution to model the onset of single layer folding:

$$\psi^{\mathrm{I}} = \left[A\mathrm{e}^{\omega z} + B\mathrm{e}^{-\omega z} + C\mathrm{e}^{\alpha\omega z} + D\mathrm{e}^{-\alpha\omega z}\right]\mathrm{e}^{\mathrm{i}\omega x} \tag{A13a}$$

$$\psi^{\mathrm{II}} = \left[A\mathrm{e}^{\omega z} + B\mathrm{e}^{-\omega z} + Cz + D\right]\mathrm{e}^{\mathrm{i}\omega x} \tag{A13b}$$

$$\psi^{\mathrm{III}} = \left[A\mathrm{e}^{\omega z} + B\mathrm{e}^{-\omega z} + C\cos(\alpha\omega z) + D\sin(\alpha\omega z)\right]\mathrm{e}^{\mathrm{i}\omega x} \tag{A13c}$$

Clearly Eq. (A8) is singular as $Wi \to ½$ (Fig. 4). This implies that nonlinear viscoelastic materials should exhibit transitional behavior in deformations where $Wi \to ½$. For example in the folding of meter thick ($H^* = 1$ m) competent beds at tectonic far field velocities ($V^* = 10^{-8}$ m/s), relaxation times τ^* (Eq. (A14)) need only be greater than about 10^7 s (~ 1 year) in order for this to occur:

$$\tau^* \geq \frac{H^*}{2V^*} = 5 \times 10^7 \text{ s} \tag{A14}$$

In this transitional region the scaling for lengths leading to Eqs. (A4a)–(A4c) cannot be expected to be valid. Fortunately, it is straightforward to deduce a new scaling factor for lengths in this case. Defining a small parameter $\sigma = \alpha^2$, assuming $0 < \sigma \ll 1$, and introducing the change of variables $\xi = x/\lambda$ into Eq. (A8), where λ is the scaling factor we seek, we obtain:

$$\frac{\sigma}{\lambda^4} \frac{\partial^4 \psi}{\partial \xi^4} + \frac{(1 + \sigma)}{\lambda^2} \frac{\partial^4 \psi}{\partial \xi^2 \partial z^2} + \frac{\partial^4 \psi}{\partial z^4} = 0. \tag{A15}$$

The scaling factor can be determined by balancing the coefficients of the first two terms in Eq. (A15). Thus:

$$\frac{\sigma}{\lambda^4} = \frac{(1 + \sigma)}{\lambda^2} \Rightarrow \lambda^2 = \frac{\sigma}{1 + \sigma} \Rightarrow \lambda \sim \sigma^{1/2} \tag{A16}$$

or

$$\xi \sim \frac{x}{\alpha}. \tag{A17}$$

Thus, the transitional behavior of this model is inversely proportional to α, i.e. the model behavior changes rapidly over distances much shorter than layer thickness. This suggests localization of deformation, perhaps at the microphysical level.

References

Alexander, J.I.D., Watkinson, A.J., 1989. Microfolding in the Permian Castile formation: an example of geometric systems in multilayer folding, Texas and New Mexico. Geological Society of America Bulletin 101, 742–750.

Batchelor, G.K., 1967. An Introduction to Fluid Dynamics. Cambridge University Press, Cambridge, UK.

Bercovici, D., Dick, H.J.B., Wagner, T.P., 1992. Nonlinear viscoelasticity and the formation of transverse ridges. Journal of Geophysical Research 97, 14195–14206.

Biot, M.A., 1961. Theory of folding of stratified viscoelastic media and its implications in tectonics and orogenesis. Geological Society of America Bulletin 72, 1595–1620.

Bull, J.M., Martinod, J., Davy, P., 1992. Buckling of the oceanic lithosphere from geophysical data and experiments. Tectonics 11, 537–548.

Chapple, W.M., 1968. A mathematical theory of finite-amplitude rock folding. Geological Society of America Bulletin 79, 47–68.

Coleman, B.D., Noll, W., 1960. An approximation theorem for functionals with applications in continuum mechanics. Archive for Rational Mechanics and Analysis 6, 355–370.

Fletcher, R.C., 1974. Wavelength selection in the folding of a single layer with power-law rheology. American Journal of Science 274, 1029–1043.

Fletcher, R.C., 1995. Three-dimensional folding and necking of a power-law layer: are folds cylindrical, and, if so, do we understand why? Tectonophysics 247, 65–83.

Goff, D.F., Wiltschko, D.V., Fletcher, R.C., 1996. Decollement folding as a mechanism for thrust ramp spacing. Journal of Geophysical Research 101, 11341–11352.

Hobbs, B.E., 1972. Deformation of non-Newtonian materials in simple shear. In: Flow and Fracture of Rocks. Geophysical Monograph Series 16. American Geophysical Union, Washington, D.C., pp. 243–258.

Hobbs, B., Muhlhaus, H.-B., Ord, A., Moresi, L.N., 2000. The influence of chemical migration upon fold evolution in multi-layered materials, in: Pohlmann, L., Krug, H.-J., Niedersen, U. (Eds.), Jahrbuch fur Komplexitat in den Natur-, Sozial- und Geisteswissenschaften, Band II. Duncker and Humblot, Berlin, pp. 229–252.

Jackson, I., 2000. Laboratory measurement of seismic wave dispersion and attenuation: recent progress, in: Karato, S.-I., Forte, A.M., Liebermann, R.C., Masters, G., Stixrude, L. (Eds.), Earth's Deep Interior: Mineral Physics and Tomography from the Atomic to the Global Scale Geophysical Monograph Series, 117. American Geophysical Union, Washington, DC, pp. 265–288.

Johnson, D., 1988. Folding and faulting in the footwall of the Diversion Thrust, north central Montana. Unpublished MS thesis, Washington State University.

Joseph, D.D., 1989. Remarks on inertial radii, persistent normal stresses, secondary motions, and nonelastic extensional viscosities. Journal of Non-Newtonian Fluid Mechanics 32 (1), 107–117.

Larson, R.G., 1992. Instabilities in viscoelastic flows. Rheologica Acta 31, 213–263.

Lin, C.C., Segel, L.A., 1994. Mathematics Applied to Deterministic Problems in the Natural Sciences. SIAM, Philadelphia.

McAdoo, D.C., Sandwell, D.T., 1985. Folding of the oceanic lithosphere. Journal of Geophysical Research 90, 8563–8569.

Mitra, S. 1986. Duplex structures and imbricate thrust systems: geometry, structural position and hydrocarbon potential. AAPG Bulletin 70 (9), 1087–1112.

Mudge, M.R., 1972. Pre-Quaternary rocks in the Sun River Canyon area, Northwestern Montana. U.S.G.S. Prof. Paper 663-A, 142pp.

Muhlhaus, H.-B., Moresi, L.N., Hobbs, B., Dufour, F., 2002. Large amplitude folding in finely layered viscoelastic rock structures. Pure and Applied Geophysics 159, 2311–2334.

Oldroyd, J.G., 1950. On the formulation of rheological equations of state. Proceedings of the Royal Society, London Series A 200, 523–541.

Parsons, B., Sclater, J.G., 1977. An analysis of the variation of ocean floor bathymetry and heat flow with age. Journal of Geophysical Research 82, 803–827.

Passman, S.L., 1982. Creep of a second-order fluid. Journal of Rheology 26 (4), 373–385.

Paterson, M.S., 1987. Problems in the extrapolation of laboratory rheological data. Tectonophysics 133, 33–43.

Patton, R.L., 1997. On the general applicability of relaxation modes in continuum models of crustal deformation. Unpublished Ph.D. thesis, Washington State University.

Patton, R.L., Manoranjan, V.S., Watkinson, A.J., 2000. Plate formation at the surface of a convecting fluid. In: Proceedings of the XIIIth International Congress on Rheology 3. British Society of Rheology, Cambridge, UK, pp. 167–169.

Ramberg, H., 1963. Fluid dynamics of viscous buckling applicable to folding of layered rocks. Bulletin of the American Association for Petroleum Geology 47, 484–505.

Rivlin, R.S., Ericksen, J.L., 1955. Stress-deformation relations for isotropic materials. Journal of Rational Mechanics and Analysis 4, 323–425.

Rundle, J.B., Passman, S.L., 1982. Constitutive laws, tensorial invariance and chocolate cake. Geophysical Surveys 5, 3–36.

Rutter, E.H., Brodie, K.H., 1991. Lithosphere rheology—a note of caution. Journal of Structural Geology 13, 363–367.

Schmalholz, S.M., Podladchikov, Y.Y., 2000. Finite amplitude folding: transition from exponential to layer length controlled growth. Earth and Planetary Science Letters 181, 619–633.

Schulson, E.M., Iliescu, D., Renshaw, C.E., 1999. On the initiation of shear faults during brittle compressive failure: a new mechanism. Journal of Geophysical Research 104, 695–705.

Segel, L.A., 1987. Mathematics Applied to Continuum Mechanics. Dover Publishers, New York.

Sherwin, J.A., Chapple, W.N., 1968. Wavelengths of single layer folds: a comparison between theory and observation. American Journal of Science 266, 167–179.

Smith, R.B., 1975. Unified theory of the onset of folding, boudinage, and mullion structure. Geological Society of America Bulletin 86, 1601–1609.

Smith, R.B., 1977. Formation of folds, boudinage, and mullion in non-Newtonian materials. Geological Society of America Bulletin 88, 312–320.

Smith, R.B., 1979. The folding of a strongly non-Newtonian layer. American Journal of Science 279, 272–287.

Spera, F.J., Borgin, A., Strimple, J., 1988. Rheology of melts and magmatic suspensions. Journal of Geophysical Research 93, 10273–10294.

Truesdell, C., 1964. The natural time of a viscoelastic fluid: its significance and measurement. Physics of Fluids 7 (8), 1134–1142.

Turcotte, D.L., Schubert, G., 2002. Geodynamics. Cambridge University Press, Cambridge.

Watkinson, A.J., Patton, R.L., 2001. Transition wavelength theory. EOS Transactions AGU, Fall Meeting Supplement 82 (47), F1195.

Zhang, Y., Hobbs, B.E., Ord, A., Muhlhaus, H.B., 1996. Computer simulation of single-layer buckling. Journal of Structural Geology 18, 643–655.